Optimal Two-Point Visual Driver Model and Controller Development for Driver-Assist Systems for Semi-Autonomous Vehicles

Changxi You[1] Panagiotis Tsiotras[2]

***Abstract*— In the research of vehicle autonomy, including the development of driver-assist systems (DAS), one important design objective is the vehicle's lateral stability during lane-tracking. This paper adopts the well-known two-point visual model to characterize the steering behavior of the driver, and investigates the optimal driver model parameters that minimize the H_2-norm of the closed-loop system. A previous study has shown that a controller based on linear multi-variable output regulator theory (ORT) has good performance and robustness characteristics during typical lane-tracking maneuvers. This paper provides limits of performance by optimizing the driver model parameters (i.e., estimating the "ideal" driver). Numerical simulations illustrate the results.**

I. INTRODUCTION

Driver modeling is an important part of modern, semi-autonomous human-vehicle-road systems [1]–[3]. A robust controller for vehicle handling stability should take into account the diverse driver habits and handling behavior of different drivers, and persistently provide good "intuitive" performance. In order to characterize driver behavior, several researchers have developed various driver models based on different methodologies [4]–[10]. All these models are able to achieve accurate lane-tracking.

This paper adopts the two-point visual driver model from [11] since it is simple, easy to use, and its parameters correspond to measurable physical variables. The two-point driver model is derived from the concept of a two-level steering mechanism observed in a series of psychological experiments using human drivers [12]–[14]. Specifically, in [12] Donges divided the driver's steering task into a guidance level and a stabilization level, and thereby built a two-level steering model. The guidance level interprets the driver's perception and response with respect to the oncoming road, and the stabilization level interprets the driver's compensatory behavior with respect to the deviation from the path. This idea has been widely accepted and has been further developed by subsequent researchers, such as [11], [13]–[16].

The current paper builds on the work of [17], but focuses on optimizing the parameters of the two-point visual driver model having in mind two objectives: (a) the optimal driver model that achieves the best lane-tracking performance, which can then be used for benchmarking; and (b) the optimal reference driver model for developing a driver-in-loop controller (DiLC). Since previous work [17] has shown that a DiLC design based on ORT (DiLC-ORT) performs better than a naïve "blending controller" in terms of the vehicle's lateral deviation from road centerline, the current paper only concentrates on improving the performance of the DiLC-ORT controller.

Section II of this paper introduces the mathematical modeling of each component in the human-vehicle-road system; Section III details the optimization methods used to find the optimal driver parameters; Section IV analyzes the results of the optimization and the numerical simulations; Finally, Section V summarizes the results of this study.

[1]C. You is a graduate student at the School of Aerospace Engineering, Georgia Institute of Technology, Atlanta. GA 30332-0150. USA. Email: cyou6@gatech.edu

[2]P. Tsiotras is a Professor at the School of Aerospace Engineering and the Institute for Robotics & Intelligent Machines, Georgia Institute of Technology, Atlanta. GA 30332-0150. USA. Email: tsiotras@gatech.edu

II. SYSTEM MODELING

The proposed human-vehicle-road system consists of four subsystems, as shown in Figure 1: the driver model, the steering column model, the vehicle model and the road and perception model.

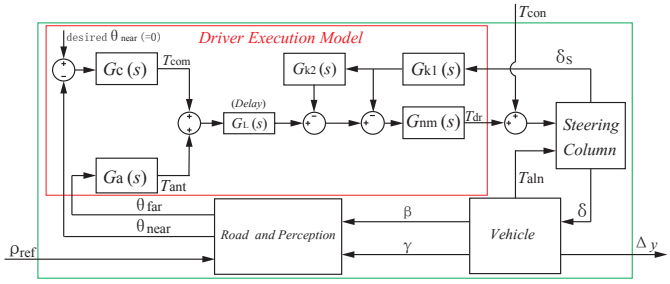

Fig. 1. Human-vehicle-road closed-loop system.

We use the same driver model, vehicle model, steering column model and the road and perception model as described in [17]. The structure of the driver model is shown in the red rectangular box in Figure 1. The transfer functions $G_{\mathrm{a}}(s)$ and $G_{\mathrm{c}}(s)$ account for the anticipatory control and the compensatory control actions of the driver, respectively. The system $G_{\mathrm{nm}}(s)$ approximately describes the neuromuscular response of the driver's arms. The "$Delay$" block indicates the driver's processing delay in the brain, and $G_{\mathrm{k1}}(s)$ and $G_{\mathrm{k2}}(s)$ account for the driver's kinesthetic perception of the steering system. The variables T_{ant} and T_{com} denote the driver's steering torques corresponding to the anticipatory control and the compensatory control paths, respectively; δ_{s} denotes the steering wheel angle; and the inputs θ_{near} and θ_{far} denote the near field and the far field visual angles, respectively (see Figure 2). Finally, T_{dr} denotes the driver's total steering torque delivered to the steering wheel. Since the removal of the kinesthetic perception feedback is not detrimental to the model accuracy and can be neglected [17],

this paper keeps this simplification in order to reduce the overall system complexity during the optimization process. The transfer functions of the blocks in Figure 1 are given below

$$G_{\rm a}(s) = K_{\rm a}, \qquad G_{\rm c}(s) = K_{\rm c}\frac{T_{\rm L}s+1}{T_{\rm I}s+1},$$
$$G_{\rm L}(s) = e^{-t_{\rm p}s}, \qquad G_{\rm nm}(s) = \frac{1}{T_{\rm N}s+1},$$

where $K_{\rm a}$ and $K_{\rm c}$ are static gains for the anticipatory and compensatory control subsystems, respectively; $T_{\rm L}$ and $T_{\rm I}$ ($T_{\rm L} > T_{\rm I}$) are lead time and lag time constants, respectively; $t_{\rm p}$ is the delay for the driver to process sensory signals and $T_{\rm N}$ is the time constant of driver's arm neuromuscular system. Figure 2 illustrates the geometric relations of the driver's visual perception, the vehicle and the road [3], [18].

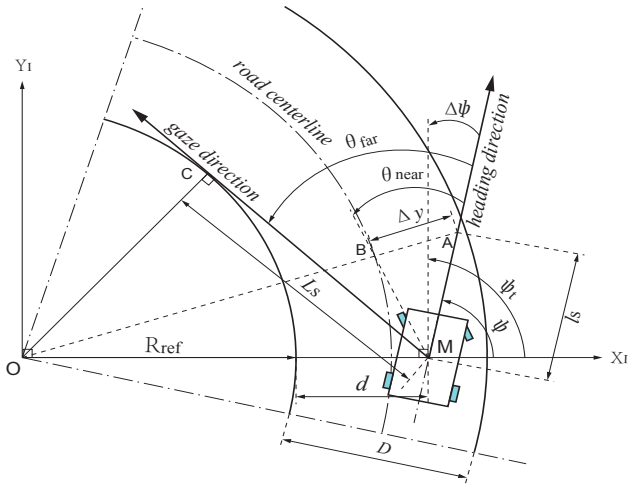

Fig. 2. Road geometries, vehicle states and driver's visual perception.

It is assumed that the vehicle is cornering with a certain lateral deviation from the road centerline. Let ψ denote the vehicle's yaw angle, let $\psi_{\rm t}$ denote the angle between the tangent to the road centerline and the $\rm X_I$ axis, let Δy denote the length of the line segment AB, and let $R_{\rm ref}$ denote the radius of the road's inner boundary. The near and far distance visual perception angles can be approximated as [3], [11], [12], [17]–[19]

$$\theta_{\rm near} \approx \frac{\Delta y}{\ell_{\rm s}}, \qquad \theta_{\rm far} \approx \frac{L_{\rm s}}{R_{\rm ref}} + \Delta\psi \approx L_{\rm s}\rho_{\rm ref} + \Delta\psi, \quad (1)$$

where $\rho_{\rm ref} = 1/R_{\rm ref}$ is the road curvature, and $\Delta\psi = \psi_{\rm t} - \psi$ is the angle difference between the tangent of the road centerline and the vehicle's heading direction.

The model of the overall vehicle-driver-perception system is summarized by

$$\dot{x} = Ax + Bu, \quad (2)$$
$$y = Cx, \quad (3)$$

where $x = (\omega_{\rm s}, \delta_{\rm s}, \beta, r, \phi, \Delta y, x_{\rm d1}, x_{\rm d2}, T_{\rm dr})^{\intercal}$, $u = \rho_{\rm ref}$ and $y = \Delta y$.

In case $T_{\rm con} \neq 0$ there is an additional input to the system, and one can redefine the augmented input as $u = (T_{\rm con}, \rho_{\rm ref})^{\intercal}$. The values of the parameters in (2)-(3) used in our problem are given in Table I.

TABLE I
SYSTEM PARAMETERS.

m	1653	kg	$V_{\rm x}$	15	m/sec
$\ell_{\rm f}$	1.402	m	$\ell_{\rm r}$	1.646	m
$L_{\rm s}$	15	m	$I_{\rm z}$	2765	$\rm kgm^2$
$J_{\rm s}$	0.11	$\rm kgm^2$	$C_{\rm f}$	42000	N/rad
$C_{\rm r}$	81000	N/rad	$b_{\rm s}$	0.57	Nm/rad/sec
$K_{\rm aln}$	359.1	Nm/rad	$g_{\rm s}$	16	–

III. PARAMETER OPTIMIZATION

This section formulates the optimization problems for two different design objectives: (a) the optimal driver parameters that achieve the smallest lane tracking error; and (b) the optimal driver parameters based on which a controller can be designed such that the vehicle's tracking error is the smallest.

For notational simplicity, let $p_1 = K_{\rm a}$, $p_2 = K_{\rm c}$, $p_3 = T_{\rm L}$, $p_4 = T_{\rm I}$, $p_5 = T_{\rm N}$, $p_6 = t_{\rm p}$ and let $p_7 = \ell_{\rm s}$. Considering the physical limits of the human driver, each model parameter lies within some given compact interval, $p_i \in [\underline{p_i},\ \overline{p_i}]$, $i = 1, 2, \ldots, 7$. Let $p = (p_1,\ p_2, \ldots,\ p_7) \in \mathbb{R}^7$, and let $\mathcal{P} = [\underline{p_1}, \overline{p_1}] \times [\underline{p_2}, \overline{p_2}] \times \cdots \times [\underline{p_7}, \overline{p_7}] \subset \mathbb{R}^7$. The partial derivative of a matrix-valued function $Z : \mathbb{R}^m \to \mathbb{R}^{n\times n}$ with respect to the vector $x \in \mathbb{R}^m$ takes the following form

$$\frac{\partial Z(x)}{\partial x} \triangleq \left[\frac{\partial Z(x)}{\partial x_1}, \frac{\partial Z(x)}{\partial x_2}, \ldots, \frac{\partial Z(x)}{\partial x_{m-1}}, \frac{\partial Z(x)}{\partial x_m}\right],$$

where x_k denotes the kth element of the vector x, where

$$\left[\frac{\partial Z(x)}{\partial x_k}\right]_{ij} = \frac{\partial Z_{ij}(x)}{\partial x_k}$$

and where $Z_{ij}(x)$ is the (i,j) entry of $Z(x)$, with $k = 1, 2, \ldots, m$ and $i, j = 1, 2, \ldots, n$.

A. Optimal Driver Parameters

First, note that system (2)-(3) is strictly proper. We need to keep the state matrix $A(p)$ in (2) Hurwitz by choosing an appropriate driver parameter vector $p \in \mathcal{P}$. Furthermore, the $\rm H_2$-norm of the system from $u = \rho_{\rm ref}$ to $y = \Delta y$ (when $T_{\rm con} = 0$) can be computed from [20]

$$\|G(s,p)\|_2^2 = {\rm tr}[CW_{\rm c}(p)C^{\intercal}], \quad (4)$$

where $G(s,p) = C(sI - A(p))^{-1}B(p)$, with $A(p)$, $B(p)$, C as in (2)-(3). $W_{\rm c}(p)$ satisfies the Lyapunov equation

$$W_{\rm c}(p)A^{\intercal}(p) + A(p)W_{\rm c}(p) + B(p)B^{\intercal}(p) = 0. \quad (5)$$

Assuming the pair $(A(p), B(p))$ is controllable for all $p \in \mathcal{P}$, it follows that $W_{\rm c}(p) > 0$ for all $p \in \mathcal{P}$. We want to solve the following optimization problem

$$\min_{p\in\mathcal{P}} \quad {\rm tr}[CW_{\rm c}(p)C^{\intercal}], \quad (6a)$$
$$\text{s.t.} \quad W_{\rm c}(p)A^{\intercal}(p) + A(p)W_{\rm c}(p) + B(p)B^{\intercal}(p) = 0, \quad (6b)$$
$$W_{\rm c}(p) > 0. \quad (6c)$$

We use a gradient descent algorithm to find the minimum value of the constrained nonlinear problem (6). To this end, let $J(p) = \mathrm{tr}[CW_{\mathrm{c}}(p)C^{\mathsf{T}}]$. The partial derivative of $J(p)$ with respect to the vector p is computed as follows

$$\frac{\partial J(p)}{\partial p} = C\frac{\partial W_{\mathrm{c}}(p)}{\partial p}(I_m \otimes C^{\mathsf{T}}), \tag{7}$$

where $W_{\mathrm{c}}(p)$ satisfies the equation in (5), and m is the length of the vector p. Note that the solution of (5) can be written as [20]

$$W_{\mathrm{c}}(p) = -\mathrm{vec}_1{}^{-1}\big([A(p)\oplus A(p)]^{-1}\mathrm{vec}_1[B(p)B^{\mathsf{T}}(p)]\big), \tag{8}$$

where $\mathrm{vec}_1 : \mathbb{R}^{n\times m} \to \mathbb{R}^{nm}$ is the vectorization operator. The matrix $A(p)\oplus A(p)$ is always invertible for all $p \in \mathcal{P}$ if the matrix $A(p)$ is Hurwitz. By taking the partial derivative of (8) with respect to the parameter vector p, one obtains

$$\begin{aligned}\frac{\partial W_{\mathrm{c}}(p)}{\partial p} &= \mathrm{vec}_1{}^{-1}\bigg(\mathrm{vec}_2\bigg(M\frac{\partial[A(p)\oplus A(p)]}{\partial p}\bigg(I_m\otimes\\ &[A(p)\oplus A(p)]^{-1}\bigg)\bigg(I_m\otimes \mathrm{vec}_1[B(p)B^{\mathsf{T}}(p)]\bigg) - M\mathrm{vec}_2^{-1}\\ &\mathrm{vec}_1\bigg(\frac{\partial B(p)}{\partial p}\bigg(I_m\otimes B^{\mathsf{T}}(p)\bigg) + B(p)\frac{\partial B^{\mathsf{T}}(p)}{\partial p}\bigg)\bigg)\bigg),\end{aligned} \tag{9}$$

where $M = [A(p)\oplus A(p)]^{-1}$, and $\mathrm{vec}_2 : \mathbb{R}^{n^2\times m} \to \mathbb{R}^{n^2 m}$ is the vectorization operator. The partial derivative of $A(p)\oplus A(p)$ with respect to p in (9) is given by

$$\begin{aligned}\frac{\partial[A(p)\oplus A(p)]}{\partial p} &= \frac{\partial[A(p)\otimes I_n]}{\partial p} + \frac{\partial[I_n\otimes A(p)]}{\partial p}\\ &= \frac{\partial A(p)}{\partial p}\otimes I_n + \bigg(I_n\otimes\frac{\partial A(p)}{\partial p}\bigg)\Psi_{m,n},\end{aligned} \tag{10}$$

where $\Psi_{m,n}$ has the form

$$\Psi_{m,n} = \begin{bmatrix} I_m\otimes e_1\otimes I_n\\ I_m\otimes e_2\otimes I_n\\ \vdots\\ I_m\otimes e_n\otimes I_n\end{bmatrix},$$

where e_k denotes the n-dimensional unit row vector, having only the kth element equal to 1 and other elements are 0.

B. Reference Driver Parameters for Controller Design

This section focuses on determining the best reference driver parameter vector p^{r} and the corresponding best DiLC-ORT controller, simultaneously.

1) Extended Closed-Loop System: Assume a fixed set of reference driver parameter vector $p^{\mathrm{r}} \in \mathcal{P}$. A DiLC-ORT controller can therefore be designed based on p^{r} following the approach of [21], with the aim of eliminating the tracking error at the near field visual point, namely,

$$\lim_{t\to\infty}\Delta y(t) = 0. \tag{11}$$

The control input T_{con} of the DiLC-ORT controller is a linear combination of a feedback term and a feedforward term,

$$T_{\mathrm{con}} = F_1(p^{\mathrm{r}})x + F_2(p^{\mathrm{r}})\rho_{\mathrm{ref}}. \tag{12}$$

Letting $B_{\mathrm{a}}(p^{\mathrm{r}}) = [B_{\mathrm{a}1},\ B_{\mathrm{a}2}(p^{\mathrm{r}})]$, the matrix $F_1(p^{\mathrm{r}})$ is chosen such that the matrix $A_{\mathrm{a}}(p^{\mathrm{r}})+B_{\mathrm{a}1}F_1(p^{\mathrm{r}})$ is Hurwitz. Then $F_2(p^{\mathrm{r}})$ is determined by solving the following equations, for some matrices $\Gamma(p^{\mathrm{r}})$ and $\Pi(p^{\mathrm{r}})$

$$F_2(p^{\mathrm{r}}) = \Gamma(p^{\mathrm{r}}) - F_1(p^{\mathrm{r}})\Pi(p^{\mathrm{r}}), \tag{13a}$$
$$A_{\mathrm{a}}(p^{\mathrm{r}})\Pi(p^{\mathrm{r}}) + B_{\mathrm{a}1}\Gamma(p^{\mathrm{r}}) + B_{\mathrm{a}2}(p^{\mathrm{r}}) = 0, \tag{13b}$$
$$C_{\mathrm{a}}\Pi(p^{\mathrm{r}}) = 0. \tag{13c}$$

Recall that $A_{\mathrm{a}}(p^{\mathrm{r}}) + B_{\mathrm{a}1}F_1(p^{\mathrm{r}})$ Hurwitz implies that there exists a positive definite matrix $P(p^{\mathrm{r}}) > 0$, such that

$$[A_{\mathrm{a}}(p^{\mathrm{r}})+B_{\mathrm{a}1}F_1(p^{\mathrm{r}})]P(p^{\mathrm{r}})+P(p^{\mathrm{r}})[A_{\mathrm{a}}(p^{\mathrm{r}})+B_{\mathrm{a}1}F_1(p^{\mathrm{r}})]^{\mathsf{T}} < 0. \tag{14}$$

Let $S(p^{\mathrm{r}}) = F_1(p^{\mathrm{r}})P(p^{\mathrm{r}})$. We then rewrite (14) as follows

$$A_{\mathrm{a}}(p^{\mathrm{r}})P(p^{\mathrm{r}}) + P(p^{\mathrm{r}})A_{\mathrm{a}}^{\mathsf{T}}(p^{\mathrm{r}}) + B_{\mathrm{a}1}S(p^{\mathrm{r}}) + S^{\mathsf{T}}(p^{\mathrm{r}})B_{\mathrm{a}1}^{\mathsf{T}} < 0.$$

The DiLC-ORT controller designed from (13) can then be designed by solving the following set of linear matrix inequalities (LMIs)

$$A_{\mathrm{a}}(p^{\mathrm{r}})P(p^{\mathrm{r}}) + B_{\mathrm{a}1}S(p^{\mathrm{r}}) + P(p^{\mathrm{r}})A_{\mathrm{a}}^{\mathsf{T}}(p^{\mathrm{r}}) + S^{\mathsf{T}}(p^{\mathrm{r}})B_{\mathrm{a}1}^{\mathsf{T}} < 0, \tag{15a}$$

$$\begin{bmatrix} -I & A_{\mathrm{a}}(p^{\mathrm{r}})\Pi(p^{\mathrm{r}}) + B_{\mathrm{a}1}\Gamma(p^{\mathrm{r}}) + B_{\mathrm{a}2}(p^{\mathrm{r}})\\ * & -\epsilon\end{bmatrix} < 0, \tag{15b}$$

$$\begin{bmatrix} -I & C_{\mathrm{a}}\Pi(p^{\mathrm{r}})\\ * & -\epsilon\end{bmatrix} < 0, \tag{15c}$$

$$P(p^{\mathrm{r}}) > 0, \tag{15d}$$

where $\epsilon > 0$ is a small infinitesimal number. After solving (15), one computes $F_1(p^{\mathrm{r}})$ from

$$F_1(p^{\mathrm{r}}) = S(p^{\mathrm{r}})P^{-1}(p^{\mathrm{r}}),$$

and then computes $F_2(p^{\mathrm{r}})$ from (13a). The extended system with the DiLC-ORT controller and a general driver in the loop, can then be represented as follows,

$$\dot{x} = \bar{A}(p,p^{\mathrm{r}})x + \bar{B}(p,p^{\mathrm{r}})u, \tag{16}$$
$$y = \bar{C}(p,p^{\mathrm{r}})x, \tag{17}$$

where the state $x \in \mathbb{R}^9$, the input $u \in \mathbb{R}$ and the output $y \in \mathbb{R}$ are the same as in the system (2)-(3). The system matrices in (16)-(17) are given as

$$\bar{A}(p,p^{\mathrm{r}}) = A_{\mathrm{a}}(p) + B_{\mathrm{a}1}F_1(p^{\mathrm{r}}), \tag{18a}$$
$$\bar{B}(p,p^{\mathrm{r}}) = B_{\mathrm{a}2}(p) + B_{\mathrm{a}1}F_2(p^{\mathrm{r}}), \tag{18b}$$
$$\bar{C}(p,p^{\mathrm{r}}) = C_{\mathrm{a}}. \tag{18c}$$

2) Optimal Reference Driver Parameters: Following the same method as in Section III.A, the H_2-norm from u to y for the extended system (16)-(17) can be determined. Since the DiLC-ORT controller is designed based on the parameters of the reference driver p^{r}, the performance of the controller will change when a different driver is operating the vehicle (i.e., $p \neq p^{\mathrm{r}}$). Thus, there may exist an optimal reference driver $p^{\mathrm{r}}_* \in \mathcal{P}$ based on which the DiLC-ORT controller can achieve better overall performance across all $p \in \mathcal{P}$. To this end, let us define an alternative parameter vector $\nu(p) = [\nu_1(p),\nu_2(p),\ldots,\nu_9(p)]^{\mathsf{T}} \in \mathbb{R}^9$ via $\nu_1 = 1/p_4, \nu_2 = 1/p_6, \nu_3 = 1/p_5, \nu_4 = p_1/p_5, \nu_5 = p_2p_3/(p_4p_6p_7), \nu_6 = p_2/(p_4p_7), \nu_7 = p_7, \nu_8 = p_2p_3/(p_7p_4^2), \nu_9 = p_1/p_6$. Note that the new parameters $\nu_1(p),\nu_2(p),\ldots,\nu_9(p)$ enter the

system matrices (2)-(3) linearly. Note also that $\nu_8 = \nu_1\nu_5/\nu_2$ and $\nu_9 = \nu_2\nu_4/\nu_3$.

Let $\nu_{17} = [\nu_1, \nu_2, \ldots, \nu_7]^\intercal \in \mathbb{R}^7$ be the new independent parameter vector, and let $p^i \in \mathcal{P}$ for $i = 1, 2, \ldots, N$ be given, where N is the number of the driver parameter models of interest. Denote by $\nu_{17}^i = \nu_{17}(p^i)$ for $i = 1, 2, \ldots, N$ the values of the new independent parameters evaluated at the driver parameters of interest, and let $\mathcal{N} = \text{co}\{\nu_{17}^1, \nu_{17}^2, \ldots, \nu_{17}^N\}$. Define the set $\mathcal{P}_c = \{p \in \mathcal{P} : \nu_{17}(p) \in \mathcal{N}\}$ and let $\underline{\nu_8}, \underline{\nu_9}$ and $\overline{\nu_8}, \overline{\nu_9}$ denote the lower and upper bounds of ν_8, ν_9 over $\mathcal{P}_c$, respectively. Finally, let $z_1 = [\nu_{17}, \underline{\nu_8}, \underline{\nu_9}]^\intercal$, $z_2 = [\nu_{17}, \underline{\nu_8}, \overline{\nu_9}]^\intercal$, $z_3 = [\nu_{17}, \overline{\nu_8}, \underline{\nu_9}]^\intercal$, $z_4 = [\nu_{17}, \overline{\nu_8}, \overline{\nu_9}]^\intercal$. Note that z_1, z_2, z_3, z_4 depend on p since ν_{17} depends on p. Furthermore, note that, by construction, $\nu_{17} \in \mathcal{N}$ whenever $p \in \mathcal{P}_c$.

Let now $G^i(s, p^\text{r}) = \bar{C}(p^i, p^\text{r})(sI - \bar{A}(p^i, p^\text{r}))^{-1}\, \bar{B}(p^i, p^\text{r})$ be the transfer function of the extended system (16)-(17) evaluated at the corresponding p^i with p^r considered as a parameter to be determined. Furthermore, let $\theta^k \in \mathbb{R}^9$ for $k = 1, 2, \ldots, 4N$ be defined by $\theta^{(j-1)N+i} = z_j(p^i)$ where $j = 1, 2, 3, 4$ and $i = 1, 2, \ldots, N$. We formulate the following optimization problem

$$\min_{p^\text{r} \in \mathcal{P}} \sum_{i=1}^{N} w_i \|G^i(s, p^\text{r})\|_2^2, \tag{19a}$$

$$\bar{A}^\intercal(\theta^k, p^\text{r})Q(p^\text{r}) + Q(p^\text{r})\bar{A}(\theta^k, p^\text{r}) < 0, \quad Q(p^\text{r}) > 0, \tag{19b}$$

$$\sum_{i=1}^{N} w_i = 1, \quad w_i \geq 0, \tag{19c}$$

where $k = 1, 2, \ldots, 4N$, and w_i are appropriate weights. We have the following theorem.

Theorem 3.1: The ORT controller resulting from (19) ensures the stability of the closed-loop system (16)-(17) for all $p \in \mathcal{P}_c$.

Proof: From (19b) it follows that the closed-loop system is stable for all $\theta \in \Theta \triangleq \text{co}\{\theta^1, \theta^2, \ldots, \theta^k\}$ and notice that $\Theta = \mathcal{N} \times [\underline{\nu_8}, \overline{\nu_8}] \times [\underline{\nu_9}, \overline{\nu_9}]$. The result follows from the fact that $p \in \mathcal{P}_c$ implies that $\nu_{17}(p) \in \mathcal{N}$ and the fact that $\nu_8(p) \in [\underline{\nu_8}, \overline{\nu_8}]$ and $\nu_9(p) \in [\underline{\nu_9}, \overline{\nu_9}]$ for all $p \in \mathcal{P}_c$.

In particular, assuming p^r is a feasible solution that satisfies the inequalities (19b) it follows that

$$\bar{A}^\intercal(\eta_i(p), p^\text{r})Q(p^\text{r}) + Q(p^\text{r})\bar{A}(\eta_i(p), p^\text{r}) < 0, \tag{20a}$$

$$Q(p^\text{r}) > 0, \tag{20b}$$

for all $i = 1, 2, \ldots, N$, where $\eta_i(p) \triangleq [\nu_{17}^i, \nu_8(p), \nu_9(p)]$ and $p \in \mathcal{P}_c$. Furthermore, note that $\eta_i(p) \in \mathcal{S}_i$, where

$$\mathcal{S}_i \triangleq \left\{ \sum_{j=1}^{4} \lambda_j \theta^{(j-1)N+i} \;\middle|\; \lambda_j \geq 0, \;\; \sum_{j=1}^{4} \lambda_j = 1 \right\}, \;\; i = 1, \ldots, N.$$

Since $\nu = [\nu_{17}, \nu_8, \nu_9]$ enters the matrices $A(\nu), B(\nu)$ (and hence also the matrices $\bar{A}(\nu, p^\text{r})$ and $\bar{B}(\nu, p^\text{r})$) linearly, it suffices to show that, given $p^\text{r} \in \mathcal{P}$, the following inequalities hold for all $\nu_{17} \in \mathcal{N}$ and for all $\nu_8 \in [\underline{\nu_8}, \overline{\nu_8}]$ and $\nu_9(p) \in [\underline{\nu_9}, \overline{\nu_9}]$

$$\bar{A}^\intercal(\nu, p^\text{r})Q(p^\text{r}) + Q(p^\text{r})\bar{A}(\nu, p^\text{r}) < 0, \tag{21a}$$

$$Q(p^\text{r}) > 0, \tag{21b}$$

which follows directly from (20a)-(20b) since ν_{17} lies in the polyhedron $\mathcal{N}$. ■

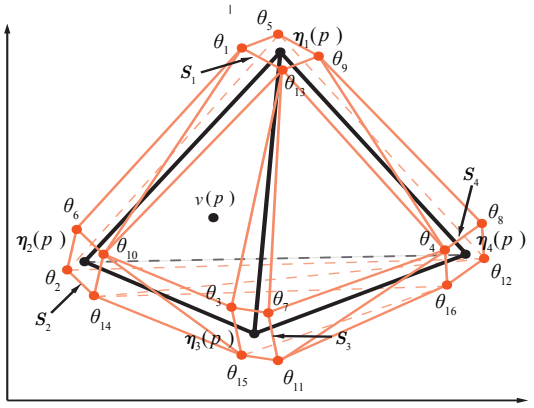

Fig. 3. Illustration of the polyhedron geometry for the case of $i = 1, 2, 3, 4$, $j = 1, 2, 3, 4$.

TABLE II

DRIVER MODEL PARAMETERS (UB=UPPER BOUNDS, LB=LOWER BOUNDS, D1=DRIVER1).

	D1	D2	D3	D4	D5	UB	LB
K_a	22	30	45	70	69.96	70	10
K_c	14	20	27	50	49.93	50	5
T_L [s]	1.6	2.4	3.5	3.03	2.29	5	0
T_I [s]	0.35	0.2	0.1	0.02	0.27	0.5	0
T_N [s]	0.12	0.12	0.12	0.01	0.12	0.2	0.01
t_p [s]	0.1	0.06	0.04	0.01	0.30	0.3	0.01
ℓ_s [m]	5	5	5	3	15	15	3

IV. Results and Analysis

Four sample drivers with different driving skills were chosen. Table II shows the parameters of these drivers. Driver1, Driver2 and Driver3 characterize the steering actions of a novice driver, a mid-skilled driver and a skilled driver, respectively. Driver4 is defined by employing the optimization results from Section III.A.

This section shows the results from the driver parameter optimization and provides a comparative analysis. The vehicle model used in all simulations is configured with Carsim 8.0 [22] and is initialized with a constant speed of 15 [m/sec](54 [km/h]). The length and the width of the road are configured as 1000 [m] and 8 [m], respectively. The road curvature is obtained through a sensor provided by Carsim.

A. Optimal Driver Model Parameters

We choose the parameters of Driver1 as the initial driver parameters, and perform the optimization following the steps outlined in equations (4)-(10). Table II provides the upper and lower bounds of each parameter and shows the optimal driver parameters (Driver4).

Except for the lead time constant T_{L}, all optimal parameters are close to their respective boundaries. These results indicate that the optimal driver spares no effort in the anticipatory/compensatory control paths, with negligibly small time delay. Figure 4 comparatively depicts the simulation results from all four drivers. In this figure, one sees that Driver3 behaves better than Driver1 and Driver2 because the parameters of Driver3 correspond to a higher driving skill; Also, as expected, Driver4 corresponding to the optimal parameters has the overall best performance. These results are validated using the H_2-norm of the closed-loop system. Table III shows the H_2-norms of the systems with different drivers, and shows that the smaller H_2-norm, the smaller the tracking error.

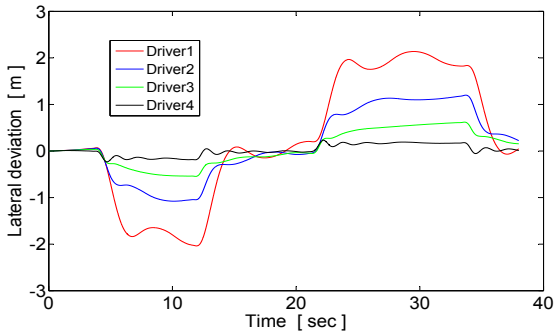

Fig. 4. Comparison of tracking errors for all four drivers.

TABLE III

H_2-NORMS REGARDING TO VARIOUS DRIVERS (D1=DRIVER1).

	D1	D2	D3	D4
H_2	275.83	145.18	108.90	33.78

B. Optimal Reference Driver Parameters

In this section we perform the iterative optimization algorithm following the procedure outlined in Section III.B. We only show the results from the balancing case, namely, when $w_i = 0.25$ for $i = 1, 2, 3, 4$. For the sake of convenience, in the following we refer to the optimal reference driver model as Driver5. Table II shows the optimal parameters of the reference driver model (D5).

To validate the optimization results, we select five reference driver models with the parameters from five distinct drivers, and design the corresponding DiLC-ORT controllers. For the sake of convenience, we call these controllers ORT1, ORT2, $\cdots$ ORT5, according to the reference driver model used in the design of each individual controller. For each of the five DiLC-ORT controllers, we place Driver1, Driver2, Driver3 and Driver4 into the loop and then calculate the H_2-norm of the closed-loop system. All the results are shown in Table IV. By comparing the results in Table III and the results in the second column of Table IV, one sees that, as expected, the H_2-norms of the systems with controller ORT1 are much smaller than that of the systems having no controller.

Figure 5 superimposes four curves from the simulations with the ORT1 and the various drivers comparing to the unassisted cases in Figure 4. These curves show that controller ORT1

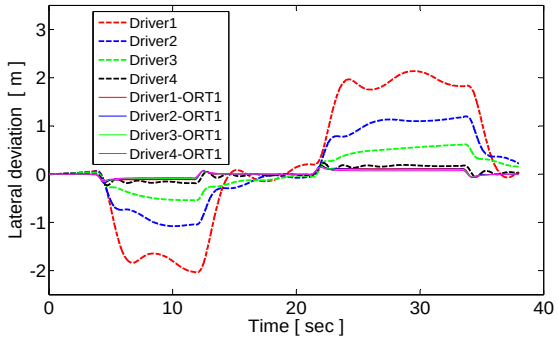

Fig. 5. Tracking errors of the systems with or without ORT controller.

improves the driver's performance significantly.

Next, we compare the performance of different controllers. The first row of Table IV shows the results when the vehicle is controlled by Driver1 and one of the five controllers, among which only ORT1 is designed based on the parameters of Driver1. In this case, controller ORT1 is expected to have the best performance since the reference driver model of ORT1 is consistent with the driver model in the loop. However, the H_2-norm of this parameter-matched system (regarded as Driver1-ORT1) is larger than that of the system with ORT2, ORT3, ORT4 and ORT5. This result implies that the optimal reference driver model for controller design is different from the driver model in the loop. To better understand this, recall that we design the DiLC-ORT controller by solving the LMIs in (15a)-(15d) and obtain a set of feasible solutions for $F_1(p^{\mathrm{r}})$ and $F_2(p^{\mathrm{r}})$. Such DiLC-ORT controller does not take into account of the H_2 performance and therefore, its H_2 performance could be further improved by tuning p^{r}. Specifically, Figure 6 illustrates the simulation results of all the parameter-matched cases and compares controller ORT5 with the other controllers. According to the curves in Figure 6, controller ORT5 has better performance than any parameter-matched controller. To explain this result, recall that we have used certain assumptions and approximations in the system modeling, which, inevitably, introduce errors into the system, and further influences the accuracy of the controller design. As a consequence, the correct driver model

TABLE IV

H_2-NORMS OF DIFFERENT COMBINATIONS OF THE DRIVERS AND THE CONTROLLERS (D1=DRIVER1).

H_2	ORT1	ORT2	ORT3	ORT4	ORT5
D1	17.49	17.32	17.15	17.12	12.95
D2	17.48	17.30	17.13	17.12	12.95
D3	17.47	17.25	17.09	17.11	12.95
D4	17.45	17.04	16.90	16.87	12.94
J_{c}	305.26	296.76	291.23	290.91	167.57

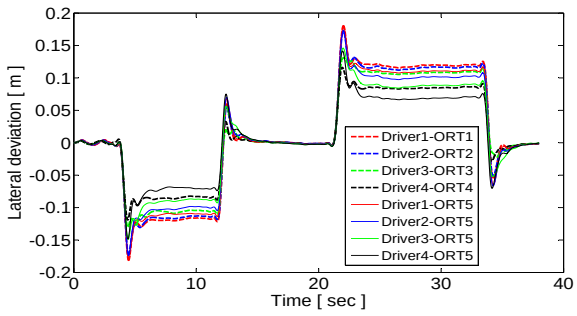

Fig. 6. Tracking errors of the parameter-matched cases comparing to the performance of ORT5.

in the loop may not provide the optimal reference for the controller.

According to the results in the last row of Table IV, controller ORT5 has the overall smallest value of the weighted objective function.

V. Conclusions

In this paper we adopt the two-point visual model to characterize driver behavior, and further improve the design of driver-in-the-loop controller (DiLC) by optimizing the driver parameters. Somewhat surprisingly, the optimization results show that the parameters of the driver model in the loop are not necessarily the best reference to design a DiLC-ORT controller. As a consequence, a methodology to design the optimal reference driver model is proposed. Both the tracking errors shown in the simulations and the H_2-norms of the corresponding closed-loop systems show that the controller based on the optimal reference driver parameters can improve driving performance significantly.

Future work will focus on better characterizing the boundaries of the driver model parameters. Although recommended values exist in the literature [23]–[26], more evidence is needed before adopting these values for optimization-based DAS designs. Also, alternative DAS control designs, beyond ORT (i.e., MPC) may be considered.

Acknowledgment

This work was supported by National Science Foundation awards CMMI-1234286 and CPS-1544814.

References

[1] A. Gray, M. Ali, Y. Gao, J. Hedrick, and F. Borrelli, "Semi-autonomous vehicle control for road departure and obstacle avoidance," *IFAC Control of Transportation Systems*, pp. 1–6, 2012.

[2] A. Gray, Y. Gao, J. K. Hedrick, and F. Borrelli, "Robust predictive control for semi-autonomous vehicles with an uncertain driver model," in *Intelligent Vehicles Symposium (IV)*. IEEE, 2013, pp. 208–213.

[3] S. Noth, I. Rañó, and G. Schöner, "Investigating human lane keeping through a simulated driver," in *Proceedings of the Driver Simulation Conference*, Paris, France, September 2012.

[4] D. H. Weir and D. T. McRuer, "Measurement and interpretation of driver steering behavior and performance," SAE Technical Paper, Tech. Rep., February 1973.

[5] C. C. MacAdam, "Application of an optimal preview control for simulation of closed-loop automobile driving," *IEEE Transactions on Systems, Man, and Cybernetics*, vol. 11, no. 6, pp. 393–399, June 1981.

[6] R. Hess and A. Modjtahedzadeh, "A control theoretic model of driver steering behavior," *IEEE Control Systems Magazine*, vol. 10, no. 5, pp. 3–8, 1990.

[7] I. Kageyama and H. Pacejka, "On a new driver model with fuzzy control," *Vehicle System Dynamics*, vol. 20, no. sup1, pp. 314–324, 1992.

[8] A. Burgett and R. Miller, "Using parameter optimization to characterize driver's performance in rear end driving scenarios," in *Proceedings: International Technical Conference on the Enhanced Safety of Vehicles*, vol. 2003. National Highway Traffic Safety Administration, 2003, pp. 21–p.

[9] Y. Lin, P. Tang, W. Zhang, and Q. Yu, "Artificial neural network modelling of driver handling behaviour in a driver-vehicle-environment system," *International Journal of Vehicle Design*, vol. 37, no. 1, pp. 24–45, 2005.

[10] M. Flad, C. Trautmann, G. Diehm, and S. Hohmann, "Individual driver modeling via optimal selection of steering primitives." Cape Town, South Africa: The Inernational Federation of Automatic Control, August 2014.

[11] C. Sentouh, P. Chevrel, F. Mars, and F. Claveau, "A sensorimotor driver model for steering control," in *IEEE International Conference on Systems, Man and Cybernetics*, San Antonio, TX, October 2009, pp. 2462–2467.

[12] E. Donges, "A two-level model of driver steering behavior," *Human Factors: The Journal of the Human Factors and Ergonomics Society*, vol. 20, no. 6, pp. 691–707, 1978.

[13] M. F. Land and D. N. Lee, "Where do we look when we steer." *Nature*, vol. 369, no. 6483, pp. 742–744, 1994.

[14] M. F. Land, "The visual control of steering," *Vision and Action*, pp. 163–180, 1998.

[15] D. D. Salvucci and R. Gray, "A two-point visual control model of steering," *Perception*, vol. 33, no. 10, pp. 1233–1248, 2004.

[16] H. Neumann and B. Deml, "The two-point visual control model of steering – new empirical evidence," in *Digital Human Modeling*. Springer, 2011, pp. 493–502.

[17] S. Zafeiropoulos and P. Tsiotras, "Design of a lane-tracking driver steering assist system and its interaction with a two-point visual driver model," in *American Control Conference*, Portland, OR, June 2014, pp. 3911–3917.

[18] I. Rano, H. Edelbrunner, and G. Schoner, "Naturalistic lane-keeping based on human driver data," in *Intelligent Vehicles Symposium (IV)*. IEEE, 2013, pp. 340–345.

[19] C. Sentouh, B. Soualmi, J. C. Popieul, and S. Debernard, "Cooperative steering assist control system," in *IEEE International Conference on Systems, Man, and Cybernetics*, Manchester, UK, October 2013, pp. 941–946.

[20] J. B. Hoagg, W. M. Haddad, and D. S. Bernstein, *Linear-Quadratic Control: Theory and Methods for Continuous-Time Systems*. Princeton University Press on Preparation.

[21] B. A. Francis, "The linear multivariable regulator problem," *SIAM Journal on Control and Optimization*, vol. 15, no. 3, pp. 486–505, 1977.

[22] *CarSim Quick Start Guide [Version 8]*, Mechanical Simulation Corporation., Ann Arbor, MI 48104, USA, June 2009.

[23] D. T. McRuer, "Human pilot dynamics in compensatory systems," DTIC Document, Wright Air Development Center, Air Research Development Command, United States Air Force, WrightPatterson Air Force Base, Dayton, OH, Tech. Rep., July 1965.

[24] D. T. McRuer and H. R. Jex, "A review of quasi-linear pilot models," *IEEE Transactions on Human Factors in Electronics*, no. 3, pp. 231–249, 1967.

[25] L. Yu, Z. Wang, and L. Qiu, "The study on pilot/flight control system and pilot model," *Electronics Optics & Control*, vol. 1, 2001.

[26] S. Horiuchi and N. Yuhara, "An analytical approach to the prediction of handling qualities of vehicles with advanced steering control system using multi-input driver model," *Journal of Dynamic Systems, Measurement, and Control*, vol. 122, no. 3, pp. 490–497, 2000.